Structural Engineering and Mechanics, Vol. 20, No. 4 (2005) 435-450
DOI: http://dx.doi.org/10.12989/sem.2005.20.4.435

Dynamic instability of functionally graded material plates subjected to aero-thermo-mechanical loads

T. Prakash†

Department of Applied Mechanics, Indian Institute of Technology Delhi, India

M. Ganapathi‡

FEA Group, Institute of Armament Technology, Girinagar, Pune-411025, India

(Received October 21, 2004, Accepted April 15, 2005)

Abstract. Here, the dynamic instability characteristics of aero-thermo-mechanically stressed functionally graded plates are investigated using finite element procedure. Temperature field is assumed to be a uniform distribution over the plate surface and varied in thickness direction only. Material properties are assumed to be temperature dependent and graded in the thickness direction according to simple power law distribution. For the numerical illustrations, silicon nitride/stainless steel is considered as functionally graded material. The aerodynamic pressure is evaluated based on first-order high Mach number approximation to the linear potential flow theory. The boundaries of the instability region are obtained using the principle of Bolotin's method and are conveniently represented in the non-dimensional excitation frequency-load amplitude plane. The variation dynamic instability width is highlighted considering various parameters such as gradient index, temperature, aerodynamic and mechanical loads, thickness and aspect ratios, and boundary condition.

Key words: functionally graded plate; forced vibration frequency; aspect ratio; temperature; gradient index; aerodynamic pressure; periodic load; instability width.

1. Introduction

Functionally graded materials (FGMs) are the new generation of composite materials in which the micro-structural details are spatially varied through non-uniform distribution of the reinforcement phase. This can be achieved by using reinforcement with different properties, sizes and shapes, as well as by interchanging the role of reinforcement and matrix phases in a continuous manner. The result is a microstructure that produces continuous change on thermal and mechanical properties at the macroscopic or continuum level. Due to recent advances in material processing capabilities, that aid in manufacturing wide variety of functionally graded materials, its use in application involving severe thermal environments is gaining acceptance in composite community, the aerospace and aircraft industry (Koizumi 1993, 1997, Suresh and Mortensen 1997, Pindera *et al.* 1994). For

† Research Scholar
‡ Professor, Corresponding author, E-mail: mganapathi@rediffmail.com

instance, in a thermal protection system, FGMs take advantage of heat and corrosion resistance typical of ceramics, and mechanical strength and toughness typical of metals. In view of these, there is an increased interest among researchers to study the dynamic behavior of the structural components made of these materials.

It is seen from the literature that the amount of work carried out on the vibration characteristics of isotropic plates and composite laminates are exhaustive. However, the investigations of FGM plates under thermo-mechanical environment are limited in number and are discussed briefly here. Tanigawa *et al*. (1996) have examined transient thermal stress distribution of FGM plates induced by unsteady heat conduction with temperature dependent material properties. Reddy and Chin (1998) have dealt with many problems, including transient response of plate due to heat flux. Senthil and Batra (2003) have carried out three-dimensional analysis of transient thermal stress in functionally graded plates adopting Laplace transformation technique and power series method. He *et al*. (2001) presented finite element formulation based on thin plate theory for the shape and vibration control of FGM plate with integrated piezoelectric sensors and actuators under mechanical load whereas Liew *et al*. (2001) have analyzed the active vibration control of plate subjected to a thermal gradient using shear deformation theory. Yang and Shen (2001) have analyzed dynamic response of thin FGM plates subjected to impulsive loads using Galerkin procedure coupled with modal superposition method whereas, by neglecting the heat conduction effect, such plates and panels in thermal environments have been examined based on shear deformation with temperature dependent material properties (Yang and Shen 2002). Cheng and Batra (2000) studied the steady state vibration of a simply supported functionally graded polygonal plate with temperature independent material properties. Sills *et al*. (2002) have presented different modeling aspects and also simulated the dynamic response under a step load.

Studies of static-stability/buckling of functionally graded plates have received its due importance in the literature (Esther and Jacob 1997, Najafizadeh and Eslami 2002, Ma and Wang 2003). However, structural components, in general, under periodic loads can undergo parametric resonance that may occur over a range of forcing frequencies and if the load is compressive to the structure, resonance or instability can usually occurs even if the magnitude of the load is below the critical buckling load of the structure. It is thus, of importance to investigate the dynamic stability of systems under periodic load (Bolotin 1964, Evan-Iwanowski 1965, Patel *et al*. 1999). Knowledge pertaining to such instability characteristics of FGM plate structure is meager in the literature and it is necessary for the optimal design and assessment of the structural failures. Ng *et al*. (2000) have investigated the parametric resonance of simply supported square FGM plates based on thin plate theory, without considering thermal and aerodynamic loads. Furthermore, the governing equations are obtained using Hamilton's principle and the solutions are determined analytically employing the assumed mode technique.

Due to the increasing utilization of FGM structural components in the design of flight vehicle structures, their stability characteristics in the presence airflow is one of the major considerations in structural design. Such investigation is scarce in the literature and the available work deals primarily with the determination of critical aerodynamic pressure of isotropic/laminated structures (Ashley and Zartarian 1956, Dixon 1966, Birman and Librescu 1990). In reality, panels may also be subjected to in-plane forces induced by edge constraints or thermal loadings, in addition to aerodynamic forces. A detailed study including the influences of thickness/aspect ratio, and aerodynamic load on the instability region is necessary for the engineers while developing structural strategies with functionally graded materials.

Here, an eight-noded shear flexible quadrilateral plate element developed based on consistency approach (Prathap *et al.* 1988, Ganapathi *et al.* 1991) is used to analyze dynamic instability behavior of aero-thermo-mechanically stressed FGM plate. The plate is further subjected to periodic in-plane mechanical load. The temperature field is assumed to be constant in the plane and varied only in the thickness direction of the plate. The material is assumed to be temperature dependent and graded in the thickness direction according to the power-law distribution in terms of volume fractions of the constituents. The aerodynamic pressure is determined based on first-order high Mach number approximation to the linear potential flow theory. A detailed investigation has been carried out to bring out the influences of thickness and aspect ratios, thermal, mechanical and aerodynamic loads and boundary condition on the dynamic instability region of functionally graded plates.

2. Theoretical development and formulation

A functionally graded rectangular plate (length a, width b, and thickness h) made of a mixture of ceramics and metals is considered with the coordinates x, y along the in-pane directions and z along the thickness direction. The material in top surface ($z = h/2$) of the plate and in bottom surface ($z = -h/2$) of the plate is ceramic and metal, respectively. The effective material properties P, such as Young's modulus E, and thermal expansion coefficient α, can be written as (Praveen and Reddy 1998)

$$P = P_c V_c + P_m V_m \tag{1}$$

where P_c and P_m are the material properties of the ceramic rich top surface and metal rich bottom surface, respectively. V_c and V_m are volume-fractions of ceramic and metal respectively and are related by

$$V_c + V_m = 1 \tag{2}$$

The properties of the plate are assumed to vary through the thickness. The property variation is assumed to be in terms of a simple power law. The volume fraction V_c is expressed as

$$V_c(z) = \left(\frac{2z+h}{2h}\right)^k \tag{3}$$

where k is the volume fraction exponent ($k \geq 0$). The material properties P that are temperature dependent can be written as

$$P = P_0(P_{-1}T^{-1} + 1 + P_1 T + P_2 T^2 + P_3 T^3) \tag{4}$$

where P_0, P_{-1}, P_1, P_2 and P_3 are the coefficients of temperature $T(K)$ and are unique to each constituent.

From Eqs. (1)-(4), the modulus of elasticity E, the coefficient of thermal expansion α, the density ρ and the thermal conductivity K are written as

$$E(z, T) = (E_c(T) - E_m(T))\left(\frac{2z+h}{2h}\right)^k + E_m(T)$$

$$\alpha(z, T) = (\alpha_c(T) - \alpha_m(T))\left(\frac{2z+h}{2h}\right)^k + \alpha_m(T)$$

$$\rho(z) = (\rho_c - \rho_m)\left(\frac{2z+h}{2h}\right)^k + \rho_m \tag{5}$$

$$K(z) = (K_c - K_m)\left(\frac{2z+h}{2h}\right)^k + K_m$$

Here the mass density ρ and thermal conductivity K are assumed to be independent of temperature. The Poisson's ratio ν is assumed to be a constant $\nu(z) = \nu_0$.

The temperature variation is assumed to occur in the thickness direction only and the temperature field is considered constant in the xy plane. In this case, the temperature through thickness is governed by the one-dimensional Fourier equation of heat conduction:

$$\frac{d}{dz}\left[K(z)\frac{dT}{dz}\right] = 0, \qquad \begin{array}{l} T = T_c \text{ and } z = h/2 \\ T = T_m \text{ and } z = -h/2 \end{array} \tag{6}$$

The solution of Eq. (6) is obtained by means of polynomial series (Wu 2004) and given by

$$T(z) = T_m + (T_c - T_m)\eta(z) \tag{7}$$

where $$\eta(z) = \frac{1}{C}\left[\left(\frac{2z+h}{2h}\right) - \frac{K_{cm}}{(k+1)K_m}\left(\frac{2z+h}{2h}\right)^{k+1} + \frac{K_{cm}^2}{(2k+1)K_m^2}\left(\frac{2z+h}{2h}\right)^{2k+1} - \right.$$

$$\left.\frac{K_{cm}^3}{(3k+1)K_m^3}\left(\frac{2z+h}{2h}\right)^{3k+1} + \frac{K_{cm}^4}{(4k+1)K_m^4}\left(\frac{2z+h}{2h}\right)^{4k+1} - \frac{K_{cm}^5}{(5k+1)K_m^5}\left(\frac{2z+h}{2h}\right)^{5k+1}\right]$$

$$C = 1 - \frac{K_{cm}}{(k+1)K_m} + \frac{K_{cm}^2}{(2k+1)K_m^2} - \frac{K_{cm}^3}{(3k+1)K_m^3} + \frac{K_{cm}^4}{(4k+1)K_m^4} - \frac{K_{cm}^5}{(5k+1)K_m^5}$$

and $K_{cm} = K_c - K_m$

Using Mindlin formulation, the displacements u, v, w at a point (x, y, z) in the plate (Fig. 1) from the medium surface are expressed as functions of mid-plane displacements u_0, v_0 and w, and independent rotations θ_x and θ_y of the normal in xz and yz planes, respectively, as

$$\begin{aligned} u(x, y, t) &= u_0(x, y, t) + z\theta_x(x, y, t) \\ v(x, y, t) &= v_0(x, y, t) + z\theta_y(x, y, t) \\ w(x, y, t) &= w(x, y, t) \end{aligned} \tag{8}$$

where t is the time. The strains in terms of mid-plane deformation can be written as

$$\{\varepsilon\} = \begin{Bmatrix} \varepsilon_p \\ 0 \end{Bmatrix} + \begin{Bmatrix} z\varepsilon_b \\ \varepsilon_s \end{Bmatrix} \tag{9}$$

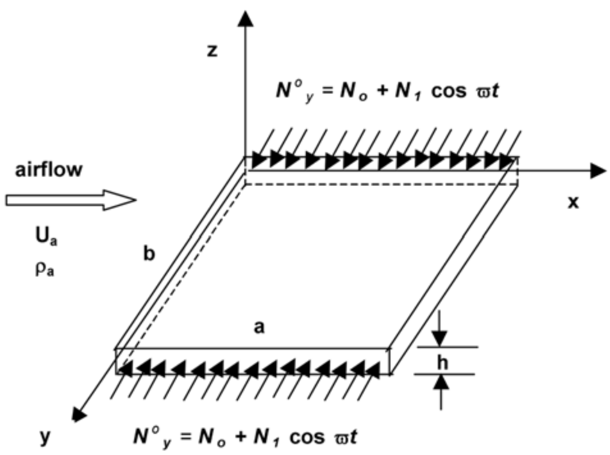

Fig. 1 Configuration and coordinate system of a rectangular FGM plate subjected to periodic in-plane load

The mid-plane strain $\{\varepsilon_p\}$, bending strains $\{\varepsilon_b\}$ and shear strains $\{\varepsilon_s\}$ in Eq. (9) are written as

$$\{\varepsilon_p\} = \begin{Bmatrix} u_{0,x} \\ v_{0,y} \\ u_{0,y} + v_{0,x} \end{Bmatrix} \tag{10}$$

$$\{\varepsilon_b\} = \begin{Bmatrix} \theta_{x,x} \\ \theta_{y,y} \\ \theta_{x,y} + \theta_{y,x} \end{Bmatrix} \tag{11}$$

$$\{\varepsilon_s\} = \begin{Bmatrix} \theta_x + w_{,x} \\ \theta_y + w_{,y} \end{Bmatrix} \tag{12}$$

where the subscript comma denotes the partial derivative with respect to the spatial coordinate succeeding it.

The membrane stress resultants $\{N\}$ and the bending stress resultants $\{M\}$ can be related to the membrane strains $\{\varepsilon_p\}$ and bending strains $\{\varepsilon_b\}$ through the constitutive relations by

$$\{N\} = \begin{Bmatrix} N_{xx} \\ N_{yy} \\ N_{xy} \end{Bmatrix} = [A_{ij}]\{\varepsilon_p\} + [B_{ij}]\{\varepsilon_b\} - \{N^T\} \tag{13}$$

$$\{M\} = \begin{Bmatrix} M_{xx} \\ M_{yy} \\ M_{xy} \end{Bmatrix} = [B_{ij}]\{\varepsilon_p\} + [D_{ij}]\{\varepsilon_b\} - \{M^T\} \tag{14}$$

where the matrices $[A_{ij}]$, $[B_{ij}]$ and $[D_{ij}]$ $(i, j = 1, 2, 6)$ are the extensional, bending-extensional coupling and bending stiffness coefficients and are defined as $[A_{ij}, B_{ij}, D_{ij}] = \int_{-h/2}^{h/2} [\overline{Q}_{ij}](1, z, z^2)dz$. The thermal stress resultant $\{N^T\}$ and moment resultant $\{M^T\}$ are

$$\{N^T\} = \begin{Bmatrix} N_x^T \\ N_y^T \\ N_{xy}^T \end{Bmatrix} = \int_{-h/2}^{h/2} [\overline{Q}_{ij}] \begin{Bmatrix} \alpha(z, T) \\ \alpha(z, T) \\ 0 \end{Bmatrix} \Delta T(z)dz \tag{15}$$

$$\{M^T\} = \begin{Bmatrix} M_x^T \\ M_y^T \\ M_{xy}^T \end{Bmatrix} = \int_{-h/2}^{h/2} [\overline{Q}_{ij}] \begin{Bmatrix} \alpha(z, T) \\ \alpha(z, T) \\ 0 \end{Bmatrix} \Delta T(z)zdz \tag{16}$$

where the thermal coefficient of expansion $\alpha(z, T)$ is given by Eq. (5), and $\Delta T(z) = T(z) - T_0$ is temperature rise from the reference temperature T_0 at which there are no thermal strains.

Similarly the transverse shear force $\{Q\}$ representing the quantities $\{Q_{xz}, Q_{yz}\}$ is related to the transverse shear strains $\{\varepsilon_s\}$ through the constitutive relations as

$$\{Q\} = [E_{ij}]\{\varepsilon_s\} \tag{17}$$

where $E_{ij} = \int_{-h/2}^{h/2} [\overline{Q}_{ij}]\kappa_i \kappa_j dz$

Here $[E_{ij}]$ $(i, j = 4, 5)$ are the transverse shear stiffness coefficients, κ_i is the transverse shear coefficient for non-uniform shear strain distribution through the plate thickness. $\overline{Q}_{ij}$ are the stiffness coefficients and are defined as

$$\overline{Q}_{11} = \overline{Q}_{22} = \frac{E(z,T)}{1-\nu^2}, \quad \overline{Q}_{12} = \frac{\nu E(z,T)}{1-\nu^2}, \quad \overline{Q}_{16} = \overline{Q}_{26} = 0, \quad \overline{Q}_{44} = \overline{Q}_{55} = \overline{Q}_{66} = \frac{E(z,T)}{2(1+\nu)} \tag{18}$$

where the modulus of elasticity $E(z, T)$ is given by Eq. (5).

The strain energy functional U is given as

$$U(\delta) = (1/2)\int_A [\{\varepsilon_p\}^T[A_{ij}]\{\varepsilon_p\} + \{\varepsilon_p\}^T[B_{ij}]\{\varepsilon_b\} + \{\varepsilon_b\}^T[B_{ij}]\{\varepsilon_p\} + \{\varepsilon_b\}^T[D_{ij}]\{\varepsilon_b\} +$$
$$\{\varepsilon_s\}^T[E_{ij}]\{\varepsilon_s\} - \{\varepsilon_p^0\}^T\{N^T\} - \{\varepsilon_b\}^T\{M^T\}]dA \tag{19}$$

where δ is the vector of the degree of freedom associated to the displacement filed in a finite element discretization.

The kinetic energy of the plate is given by

$$\overline{T}(\delta) = (1/2)\int_A [p(\dot{u}_0^2 + \dot{v}_0^2 + \dot{w}_0^2) + I(\dot{\theta}_x^2 + \dot{\theta}_y^2)]dA \tag{20}$$

where $p = \int_{-h/2}^{h/2} \rho(z)dz$, $I = \int_{-h/2}^{h/2} z^2\rho(z)dz$ and $\rho(z)$ is mass density which varies through the thickness of the plate and is given by Eq. (5). The dot over the variables denotes in Eq. (20) the derivative with respect to time.

The plate is subjected to temperature filed and this, in turn, results in-plane stress resultants $(N_{xx}^{th}, N_{yy}^{th}, N_{xy}^{th})$. Thus, the potential energy due to pre-buckling stresses $(N_{xx}^{th}, N_{yy}^{th}, N_{xy}^{th})$ developed under thermal load can be written as

$$V(\delta) = \int_A \left\{ \frac{1}{2}\left[N_{xx}^{th}\left(\frac{\partial w}{\partial x}\right)^2 + N_{yy}^{th}\left(\frac{\partial w}{\partial y}\right)^2 + 2N_{xy}^{th}\left(\frac{\partial w}{\partial x}\right)\left(\frac{\partial w}{\partial y}\right)\right]\right.$$

$$\left. + \frac{h^3}{24}\left[N_{xx}^{th}\left\{\left(\frac{\partial \theta_x}{\partial x}\right)^2 + \left(\frac{\partial \theta_y}{\partial x}\right)^2\right\} + N_{yy}^{th}\left\{\left(\frac{\partial \theta_x}{\partial y}\right)^2 + \left(\frac{\partial \theta_y}{\partial y}\right)^2\right\} + 2N_{xy}^{th}\left\{\left(\frac{\partial \theta_x}{\partial x}\right)\left(\frac{\partial \theta_x}{\partial y}\right) + \left(\frac{\partial \theta_y}{\partial x}\right)\left(\frac{\partial \theta_y}{\partial y}\right)\right\}\right]\right\} dA \quad (21)$$

The potential energy due to external in-plane mechanical forces, N_y^o in y direction is written as,

$$W(\delta) = \frac{1}{2}\int N_y^o[\partial w/\partial y]^2 dA \quad (22)$$

The work done by the applied non-conservative load is

$$W_a(\delta) = \int_A \Delta p w dA \quad (23)$$

where Δp is the aerodynamic pressure. The aerodynamic pressure based on first-order, high Mach number approximation to the linear potential flow (Ashley and Zartarian 1956) is

$$\Delta p = \frac{\rho_a U_a^2}{\sqrt{M_\infty^2 - 1}}\left[\frac{\partial w}{\partial x} + \left(\frac{1}{U_a}\right)\frac{M_\infty^2 - 2}{M_\infty^2 - 1}\frac{\partial w}{\partial t}\right] \quad (24)$$

where ρ_a, U_a and M_∞ are the free stream air density, velocity and Mach number, respectively. Further, it has been shown by Dixon (1966) that the two-dimensional static aerodynamic approximation provides results that are in complete agreement with those based on exact aerodynamic theories for Mach numbers between $\sqrt{2}$ and 2. The aerodynamic pressure for high supersonic speed, within the 2D static approximation, neglecting the aerodynamic damping is given as (Birman and Librescu 1990)

$$\Delta p = \frac{\rho_a U_a^2}{\sqrt{M_\infty^2 - 1}}\left[\frac{\partial w}{\partial x}\right] \quad (25)$$

Substituting Eqs. (19)-(25) in Lagrange's equation of motion, one obtains the governing equations as

$$[M]\{\ddot{\delta}\} + ([K] + [K_G]^{th} + N_y^o[K_G]^m + \lambda[\bar{A}])\{\delta\} = 0 \quad (26)$$

where $[K]$ and $[M]$ are stiffness matrix and the consistent mass matrix; $\{\ddot{\delta}\}$ is the acceleration vector. $[K_G]^{th}$ & $[K_G]^m$ are geometric stiffness matrices due to thermal and mechanical loads; $[\bar{A}]$ is the aero-dynamic force. Here $\lambda\left(= \frac{\rho_a U_a^2}{\sqrt{M_\infty^2 - 1}}\right)$ refers the aerodynamic pressure.

3. Parametric instability analysis

The state of periodic load is the uniform pulsating axial compressive force N_y^o, which may be defined as

$$N_y^o = (N_o + N_1\cos\bar{\omega}t) = (\bar{\alpha} + \beta\cos\bar{\omega}t)N_{cr}^o \tag{27}$$

where, $\bar{\alpha} = N_o/N_{cr}^o$, $\beta = N_1/N_{cr}^o$, N_{cr}^o, $\bar{\omega}$ are static buckling load of the plate and the frequency of the dynamic in-plane load, respectively. From Eqs. (23) and (24), we have the governing equation of the form

$$[M]\{\ddot{\delta}\} + [[K] + [K_G]^{th} + \lambda[\bar{A}] + (\bar{\alpha}N_{cr}^o + \beta N_{cr}^o\cos\bar{\omega}t)[K_G]^m]\{\delta\} = \{\mathbf{o}\} \tag{28}$$

Eq. (28) represents the dynamic stability problem of a system subjected to a periodic in-plane axial force. The dynamic instability boundary is determined using the method suggested in the literature (Bolotin 1964, Evan-Iwanowski 1965, Patel *et al.* 1999). To obtain points on the boundaries of the instability region, the components $\{\delta\}$ are written in the Fourier series as

$$\{\delta\} = \frac{1}{2}\{\mathbf{b}\}_0 + \sum_{i=2,4,6,\ldots}\left[\{\mathbf{a}\}_i\sin\left(\frac{i\bar{\omega}t}{2}\right) + \{\mathbf{b}\}_i\cos\left(\frac{i\bar{\omega}t}{2}\right)\right] \tag{29}$$

with period T, where $T = 2\pi/\bar{\omega}$, or

$$\{\delta\} = \sum_{i=1,3,5,\ldots}\left[\{\mathbf{a}\}_i\sin\left(\frac{i\bar{\omega}t}{2}\right) + \{\mathbf{b}\}_i\cos\left(\frac{i\bar{\omega}t}{2}\right)\right] \tag{30}$$

with period $2T$. These expressions are substituted in the Eq. (28) and the coefficients of each sine and cosine terms are set equal to zero, as well as the sum of the constant terms. For nontrivial solutions, the determinants of the coefficients of these groups of linear homogeneous equations are equal to zero. The problem is now reduced to that of finding the eigenvalues of the systems. Using the standard eigenvalue extraction scheme, for the given value of $\bar{\alpha}$, the variation of the eigenvalues $\bar{\omega}$ with respect to β can be found out. The plot of such variation in $\beta - \bar{\omega}$ plane shows the instability regions associated with the given plate subjected to harmonically excited in-plane load.

4. Element description

The plate element employed here is a C^0 continuous shear flexible element and needs five nodal degrees of freedom u_0, v_0, w, θ_x, θ_y at eight nodes in QUAD-8 element. If the interpolation functions for QUAD-8 are used directly to interpolate the five variables u_0 to θ_y in deriving the shear strains and membrane strains, the element will lock and show oscillations in the shear and membrane stresses. Field consistency requires that the transverse shear strains and membrane strains must be interpolated in a consistent manner. Thus θ_x and θ_y terms in the expressions for $\{\varepsilon_s\}$ given by Eq. (12) have to be consistent with field functions $w_{,x}$ and $w_{,y}$. This is achieved by using field redistributed substitute shape functions to interpolate those specific terms, which must be consistent, as described in the literature (Prathap *et al.* 1988, Ganapathi *et al.* 1991). This element is free from locking syndrome and has good convergence properties. For the sake of brevity, these are not presented here, as they are available in the literature (Prathap *et al.* 1988, Ganapathi *et al.* 1991). Since the element is based on field consistency approach, exact integration is applied for calculating various strain energy terms.

5. Results and discussion

In this section, we use the above formulation to investigate the effect of parameters like gradient index, aspect and thickness ratios, aerodynamic pressure and thermal gradient on the dynamic instability of functionally graded plates subjected to periodic in-plane mechanical load. Based on progressive mesh refinement, 8 × 8 mesh idealization is found to be adequate to model the full plate for the present analysis. Fig. 2 shows the variation of the volume fractions of ceramic and metal respectively, in the thickness direction z for the FGM plate. The top surface is ceramic rich and the bottom surface is metal rich. The FGM plate considered here consists of Silicon nitride (Si_3N_4) and stainless steel (SUS304). The temperature coefficients corresponding to Si_3N_4/SUS304 are listed in Table 1 (Reddy and Chin 1998). The mass density and thermal conductivity are: $\rho_c = 2370$ kg/m^3, $K_c = 9.19$ W/mK for Si_3N_4; and $\rho_m = 8166$ kg/m^3, $K_m = 12.04$ W/mK for SUS304. Poisson's ratio ν is assumed to be a constant and equals to 0.28. Transverse shear coefficient is taken as 0.91. The plate is of uniform thickness and boundary conditions considered here are:

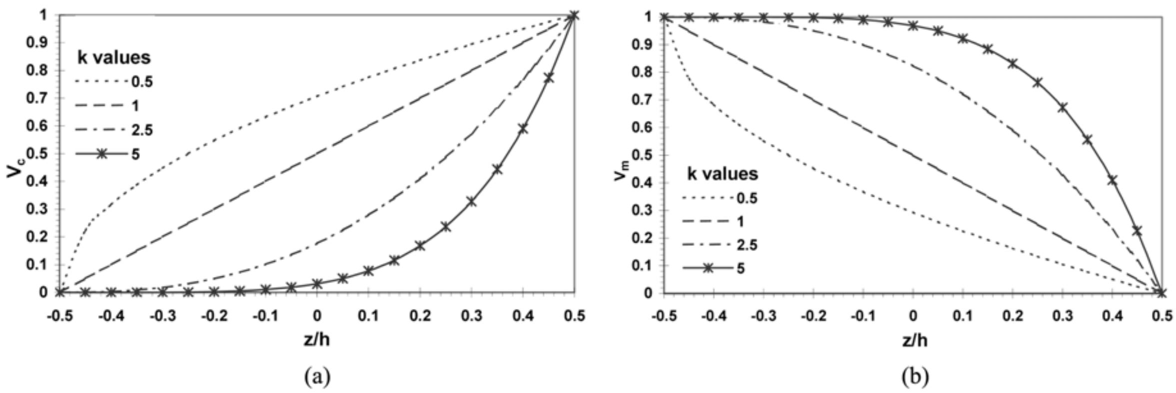

Fig. 2 Variation of volume fractions through thickness: a) Ceramic; b) Metal

Table 1 Temperature dependent coefficients for material Si_3N_4/SUS304 (Reddy and Chin 1998)

Materials	Properties	P_0	P_{-1}	P_1	P_2	P_3	P (T = 300K)
Si_3N_4	E (Pa)	348.43e+9	0.0	−3.070e-4	2.160e-7	−8.946e-11	322.2715e+9
	α (1/K)	5.8723e-6	0.0	9.095e-4	0.0	0.0	7.4746e-6
SUS304	E (Pa)	201.04e+9	0.0	3.079e-4	−6.534e-7	0.0	207.7877e+9
	α (1/K)	12.330e-6	0.0	8.086e-4	0.0	0.0	15.321e-6

simply supported :

$$u = w = \theta_y = 0 \text{ on } x = 0, a \quad \text{and} \quad v = w = \theta_x = 0 \text{ on } y = 0, b$$

clamped support :

$$u = v = w = \theta_x = \theta_y = 0 \text{ on } x = 0, a \quad \& \quad y = 0, b$$

Before proceeding for the detailed analysis, the formulation developed herein is validated by considering the linear free vibration and thermal buckling analyses of FGM plates. Tables 2(a) and 2(b) show the natural frequencies as well as critical thermal buckling temperature of FGM plates and are compared with the available solutions (Huang and Shen 2004, Wu 2004). Here, the calculated non-dimensional linear frequency and the critical temperature difference are defined a $\bar{\Omega}\left(= \omega\left(\frac{a^2}{h}\right)\left(\frac{\rho_m(1-\nu^2)}{E_m}\right)^{(1/2)}\right)$, and ΔT_{cr} (= $T_c - T_m$) between the surfaces. ρ_m and E_m are the mass density and Young's modulus of metal, respectively.

Table 2(a) Comparison of non-dimensional frequencies ($\bar{\Omega}_{ij}$) of simply supported FGM plate (a/b = 1, a/h = 8)

Temperature	k	Frequencies					
		$\bar{\Omega}_{11}$		$\bar{\Omega}_{12}$		$\bar{\Omega}_{13}$	
		Huang and Shen (2004)	Present	Huang and Shen (2004)	Present	Huang and Shen (2004)	Present
T_c = 400, T_m = 300	0.0	12.397	12.311	29.083	29.016	43.835	44.094
	0.5	8.615	8.483	20.215	19.979	30.530	30.391
	1.0	7.474	7.444	17.607	17.511	26.590	26.648
	2.0	6.693	6.679	15.762	15.706	23.786	23.894
	10.0	---	5.742	---	13.560	---	20.609
T_c = 600, T_m = 300	0.0	11.984	11.888	28.504	28.421	43.107	43.343
	0.5	8.269	8.150	19.784	19.534	29.998	29.836
	1.0	7.171	7.131	17.213	17.101	26.109	26.139
	2.0	6.398	6.376	15.384	15.314	23.327	23.410
	10.0	---	5.423	---	13.146	---	20.100

Table 2(b) Critical buckling temperature difference (ΔT_{cr}) of simply supported aluminum-alumina FGM plate (a/h = 10, Tm = 5 deg, free to move in-plane)

k		a/b = 1	a/b = 2	a/b = 3	a/b = 4	a/b = 5
0	Present	3259.915	7648.325	13847.425	20774.597	27600.137
	Wu (2004)	3256.310	7640.640	13835.530	20760.850	27586.740
1	Present	1978.512	4696.518	8627.139	13150.701	17749.685
	Wu (2004)	1976.297	4691.691	8619.424	13141.430	17740.250
5	Present	1482.941	3481.831	6294.315	9421.755	12487.570
	Wu (2004)	1481.297	3478.338	6288.939	9415.583	12481.590

It is observed from these Tables that the present results agree very well with the existing literature. It is further revealed from Table 2(a) that, with the increase in power law index k up to certain value, the rate of decrease in the frequency value is high, and further increase in k leads to less reduction in the frequency. For the high values of k, the stiffness degradation occurs due to the increase in the metallic volumetric fraction. Here, in view of the computational time involved for the parametric resonance analysis, one term solution of Eq. (28) is employed, which furnishes accurate results for the low values of load amplitude. Furthermore, the analysis is focused mainly on the determination of boundaries of the primary instability region that occurs in the vicinity of simple resonance of first order, 2 ω_i (ω_i is the ith the natural frequency where i = 1, 2, 3...) which is by far the largest one compared to the neighborhood of combination resonance of first order, ($\omega_i \pm \omega_j$). This is the most dangerous zone and has the greatest practical importance (Bolotin 1964, Evan-Iwanowski 1965, Patel *et al.* 1999).

Next, the dynamic instability of square plates (a/b = 1, a/h = 20) is studied considering mechanically /thermally/aerodynamically pre-stressed functionally graded plates and the results obtained are plotted in Fig. 3. Here, the plot of primary instability region in the neighborhood of 2 ω_i in terms of non-dimensional excitation frequencies, $\Omega\left(=\bar{\omega}\left(\frac{a^2}{h}\right)\left(\frac{12\rho_m(1-\nu^2)}{E_m}\right)^{(1/2)}\right)$ versus the dynamic in-plane

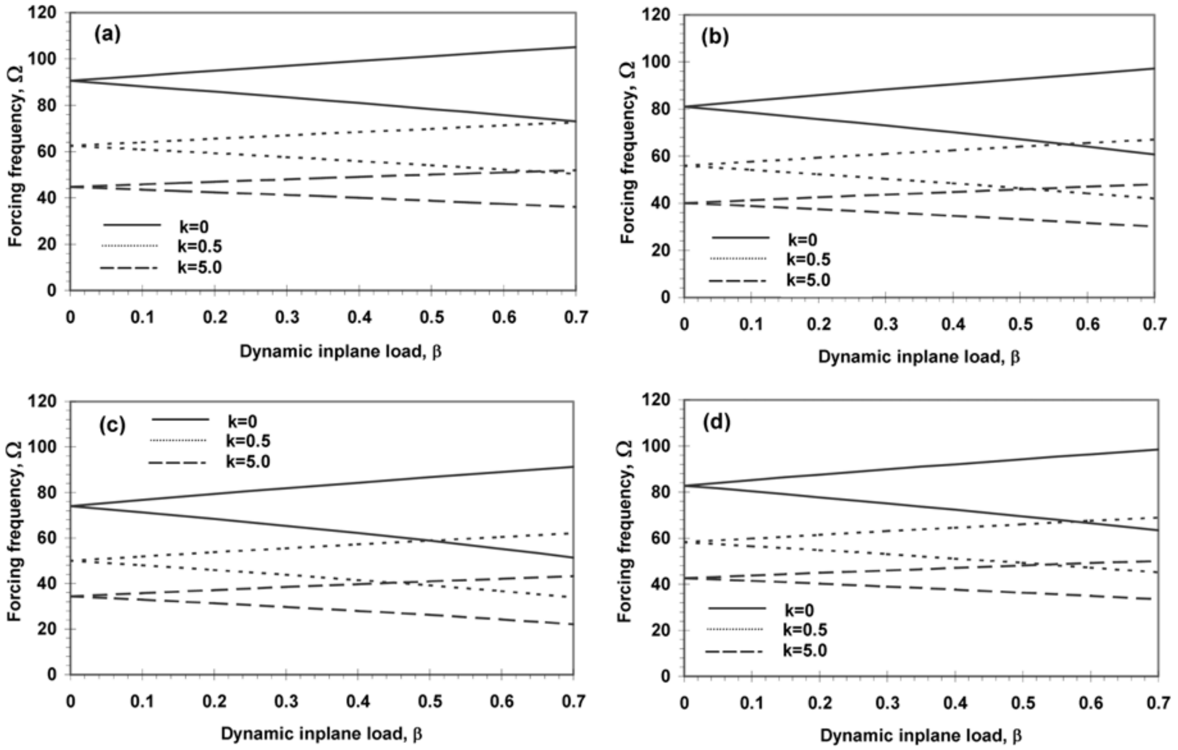

Fig. 3 Instability region versus dynamic in-plane load amplitude of a simply supported FGM plate (a/b = 1, a/h = 20) with different gradient index: (a) $\bar{\alpha}$ = 0, T_c = 300, T_m = 300, λ = 0; (b) $\bar{\alpha}$ = 0.2, T_c = 300, T_m = 300, λ = 0; (c) $\bar{\alpha}$ = 0.2, T_c = 400, T_m = 300, λ = 0; (d) $\bar{\alpha}$ = 0.2, T_c = 400, T_m = 300, λ = 200

load β are depicted. The width of primary instability $\Delta\Omega$ is the separation of the boundaries of the primary instability region for the given plate. This can be used as an instability measure to study the influence of other parameters. It is observed from Fig. 3(a) that, with the increase in the value of gradient index k, the origin of instability shifted to lower forcing frequency, and the width of the instability region decreases for the given dynamic load amplitude β. The instability zone in general increases with dynamic load amplitude. Furthermore it is noticed that the boundaries of the instability regions with respect to gradient index k overlap at higher dynamic load, leading to wide range of operating frequency under which the system becomes unstable. It is also revealed from Figs. 3(b) and (c) that the variation of parametric resonance zone of mechanically/thermally pre-stressed FGM plate is qualitatively similar to those of without pre-stressed case. However, the presence of compressive nature of in-plane loads resulting from statically applied mechanical and thermal field, further enlarge the dangerous zone and occurs at low operating frequency. The influence of aerodynamic force is rather to reduce the instability region and postpone the occurrence of resonance to higher forcing frequency value as inferred from Fig. 3(d) and the overlap of instability zone with k occurs at higher amplitude compared to those of without airflow case.

Fig. 4 highlights the influences of aspect ratio of FGM plate on the unstable operating frequency range. It is viewed that the origin of unstable zone is shifted to higher frequency with the increase in the aspect ratio. However, for the given gradient index, it can be noted that the width of instability zone increases with aspect ratio. As the aspect ratio increases, the origin of instability is closer for higher ingredient index compared to the lower k value. The effect of thickness ratio is also examined and is shown in Fig. 5 for different values of gradient index. It can be inferred from

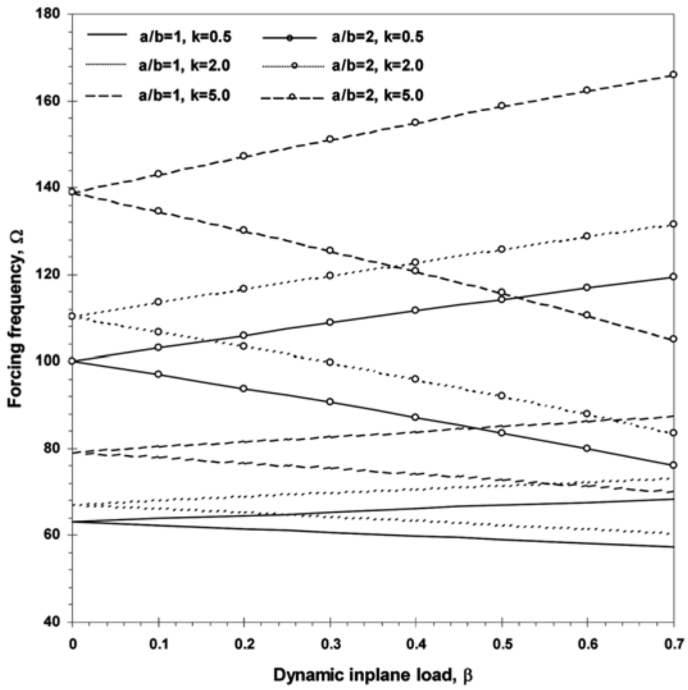

Fig. 4 Effect of aspect ratio on the instability region with dynamic in-plane load amplitude of a simply supported FGM Plate ($a/h = 20$) with different gradient index ($\overline{\alpha} = 0.2$, $T_c = 400$, $T_m = 300$, $\lambda = 400$)

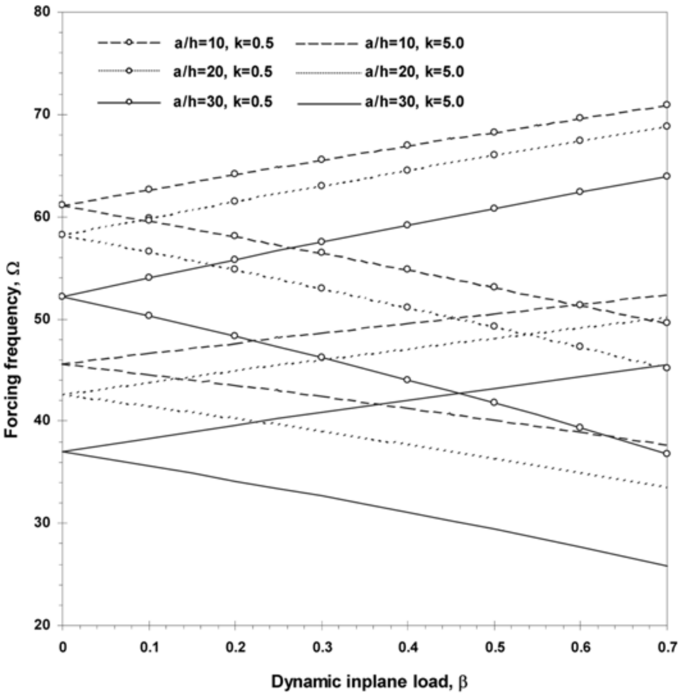

Fig. 5 Effect of thickness ratio on the instability region with dynamic in-plane load amplitude of a simply supported square FGM Plate with different gradient index ($\overline{\alpha}$ = 0.2, T_c = 400, T_m = 300, λ = 200)

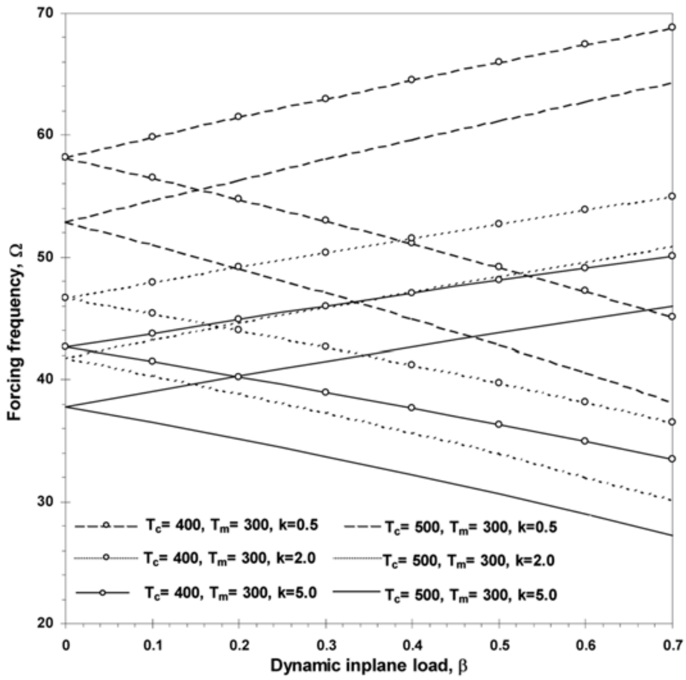

Fig. 6 Effect of temperature on the instability region with dynamic in-plane load amplitude of a simply supported FGM Plate (a/b = 1, a/h = 20) with different gradient index ($\overline{\alpha}$ = 0.2, λ = 200)

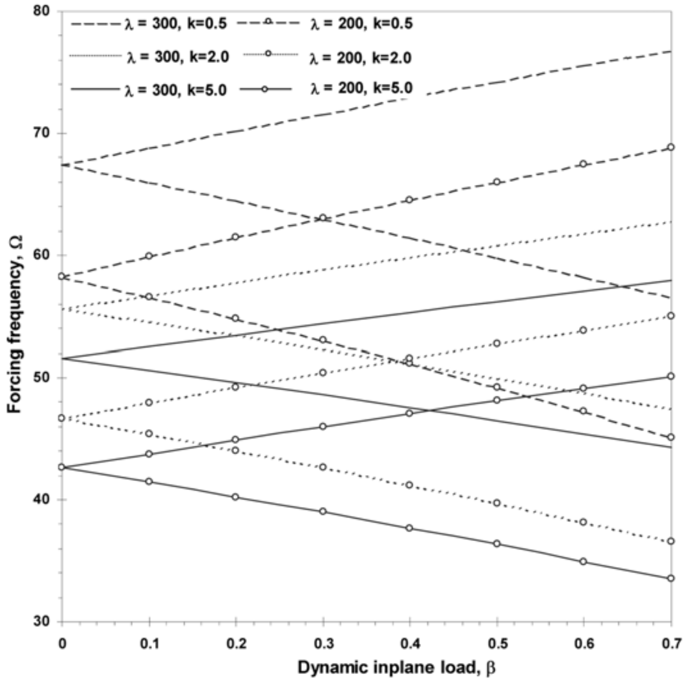

Fig. 7 Effect of aerodynamic pressure on the instability region with dynamic in-plane load amplitude of a simply supported FGM Plate ($a/b = 1$, $a/h = 20$) with different gradient index ($\overline{\alpha} = 0.2$, $T_c = 400$, $T_m = 300$)

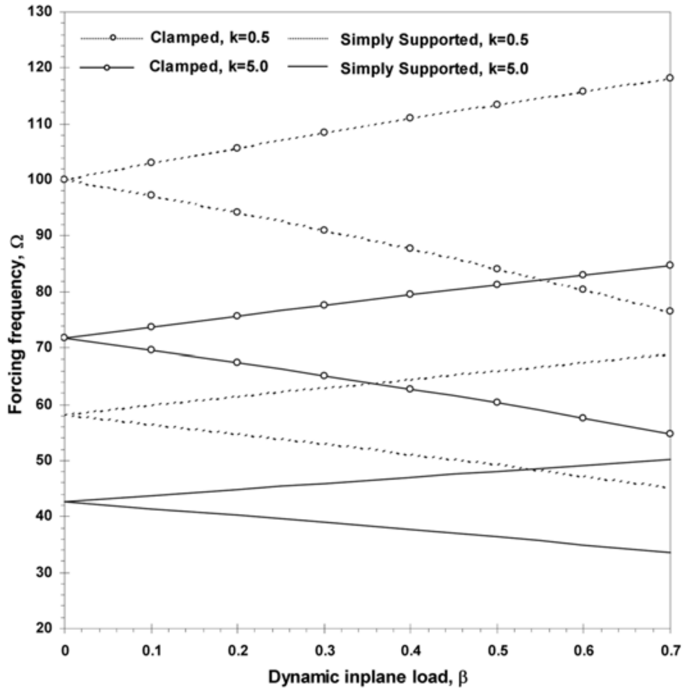

Fig. 8 Effect of boundary condition on the instability region with dynamic in-plane load amplitude of a FGM Plate ($a/b = 1$, $a/h = 20$) with different gradient index ($\overline{\alpha} = 0.2$, $T_c = 400$, $T_m = 300$, $\lambda = 200$)

Fig. 5 that, with the increase in thickness, the instability initiates at higher operating frequency and yields low frequency band for the system to be unstable. For the low value of k, overlap in the instability regions occurs relatively at low dynamic load amplitude while increasing the thickness.

Finally, Fig. 6 describes the influence of thermal gradient on the dynamic instability of FGM plate. It can be noted that, with the increase in the surface temperature difference, the origin of instability is shifted to lower frequency and the unstable frequency width is more, as expected. The effect of aerodynamic load on the parametric resonance is investigated and given in Fig. 7. It is observed that it enhances the stability strength by shifting the origin of unstable region to higher operating value and reducing the width of the instability. For low k, the overlap of unstable region occurs at low load amplitude while increasing the aerodynamic pressure. The effect of boundary condition is also studied and exhibited in Fig. 8. It can be seen that the origin of instability as well as the width of the unstable region are high for clamped case compared to simply supported case.

6. Conclusions

Parametric instability study of aero-thermo-mechanically pre-stressed functionally graded plates, subjected periodic in-plane load, is examined using eight-noded plate element based on first-order shear flexible theory. Numerical results have been obtained various geometric parameters, boundary condition and gradient index. From the detailed study, the following observations can be made:

i) With the increase in the value of gradient index, the origin of the primary dynamic instability region shifts to lower excitation frequencies and decreases the width of the unstable excitation frequency range.
ii) At higher amplitude of load, the dynamic stability regions overlap with the increase in the value of gradient index.
iii) The effect high thermal gradient is to destabilize the system at lower excitation frequency as expected.
iv) Unlike the pre-stressed cases of mechanical and thermal, the aerodynamic pressure load enhances the stability strength by shifting the origin of instability to higher value and reducing the width of operating frequency range.
v) The increase in the aspect ratio and rigidity of the support results in shifting the origin of in stability to higher frequency and remains unstable for wide range of excitation frequency.
vi) With the increase in aspect ratio, the origins of instability are closer for higher ingredient index.
vii) With increase in thickness, the instability is postponed to higher forcing frequency, and the overlap in the instability regions occurs relatively at low dynamic load amplitude.

References

Ashley, H. and Zartarian, G. (1956), “Piston theory – a new aerodynamic tool for the aeroelastician”, *J. Aeronaut Sci.*, **12**, 1109-1118.

Birman, V. and Librescu, L. (1990), “Supersonic flutter of shear deformation laminated flat panel”, *J. Sound Vib.*, **139**, 265-275.

Bolotin, V.V. (1964), *The Dynamic Stability of Elastic Systems*, Holden-Day, San Francisco.

Cheng, Z.Q. and Batra, R.C. (2000), “Three dimensional thermoelastic deformations of a functionally graded

elliptic plate", *Compos. Part B: Engg.,* **31**, 97-106.
Dixon, S.C. (1966), "Comparison of panel flutter results from approximate aerodynamic theory with results from exact theory and experiment", *NASA* TN D-3649.
Evan-Iwanowski, R.M. (1965), "On the parametric response of structures", *Appl. Mech. Rev.*, **18**, 699-702.
Feldman, E. and Aboudi, J. (1997), "Buckling analysis of functionally graded plates subjected to thermal loading", *Compos. Struct.*, **38**, 29-36.
Ganapathi, M., Varadan, T.K. and Sarma, B.S. (1991), "Nonlinear flexural vibrations of laminated orthotropic plates", *Comput. Struct.*, **39**, 685-688.
He, X.Q., Ng, T.Y., Sivashankar, S. and Liew, K.M. (2001), "Active control of FGM plates with integrated piezoelectric sensors and actuators", *Int. J. Solids Struct.,* **38**, 1641-1655.
Huang, X.L. and Shen, H.S. (2004), "Nonlinear vibration and dynamic response of functionally graded plates in thermal environments", *Int. J. Solids Struct.,* **41**, 2403-2427.
Koizumi, M. (1993), "The concept of FGM", *Ceram. Trans Functionally Graded Material*, **34**, 3-10.
Koizumi, M. (1997), "FGM activities in Japan", *Composites*, **28**, 1-4.
Liew, K.M., He, X.Q., Ng, T.Y. and Sivashankar, S. (2001), "Active control of FGM plates subjected to a temperature gradient : Modeling via finite element method based on FSDT", *Int. J. Numer. Methods Engg.,* **52**, 1253-1271.
Ma, L.S. and Wang, T.J. (2003), "Nonlinear bending and post-buckling of a functionally graded circular plate under mechanical and thermal loadings", *Int. J. Solids Struct.,* **40**, 3311-3330.
Najafizadeh, M.M. and Eslami, M.R. (2002), "First order theory based thermoelastic stability of functionally graded materials circular plates", *AIAA J,* **40**, 1444-1450.
Ng, T.Y., Lam, K.Y. and Liew, K.M. (2000), "Effect of FGM materials on parametric response of plate structures", *Comput. Methods Appl. Mech. Engg.*, **190**, 953-962.
Patel, B.P., Ganapathi, M., Prasad, K.R. and Balamurugan, V. (1999), "Dynamic instability of layered anisotropic composite plates on elastic foundations", *Engg. Struct.*, **21**, 988-995.
Pindera, M.J., Arnold, S.M., Aboudi, J. and Hui, D. (1994), "Use of composites in functionally graded materials", *Compos. Engng.,* **4**, 1-145.
Prathap, G., Naganarayana, B.P. and Somashekar, B.R. (1988), "A field consistency analysis of the isoparametric eight-noded plate bending elements", *Comput. Struct.*, **29**, 857-874.
Praveen, G.N. and Reddy, J.N. (1998), "Nonlinear transient thermoelastic analysis of functionally graded ceramic-metal plates", *Int. J. Solids Struct.,* **35**, 4457-4476.
Reddy, J.N. and Chin, C.D. (1998), "Thermomechanical analysis of functionally graded cylinders and plates", *J. Therm. Stresses*, **21**, 593-629.
Senthil, S. Vel and Batra, R.C. (2003), "Three-dimensional analysis of transient thermal stresses in functionally graded plates", *Int. J. Solids Struct.,* **40**, 7181-7196.
Sills, L.B., Eliaso, R. and Berlin, Y. (2002), "Modeling of functionally graded materials in dynamic analyses", *Compos. Part B: Engg.,* **33**, 7-15.
Suresh, S. and Mortensen, A. (1997), "Functionally graded metals and metal-ceramic Composites - Part 2. Thermomechanical behavior", *Int. Mater. Rev.*, **42**, 85-116.
Tangiawa, Y., Akai, T., Kawamura, R. and Oka, N. (1996), "Transient heat conduction and thermal stress problems of a nonhomogeneous plate with temperature-dependent material properties", *J. Therm. Stresses*, **19**, 77-102.
Wu, L. (2004), "Thermal buckling of a simply supported moderately thick rectangular FGM plate", *Compos. Struct.*, **64**, 211-218.
Yang, J. and Shen, H.S. (2001), "Dynamic response of initially stressed functionally graded rectangular thin plates", *Compos. Struct.*, **54**, 497-508.
Yang, J. and Shen, H.S. (2002), "Vibration characteristic and transient response of shear-deformable functionally graded plates in thermal environments", *J. Sound Vib.*, **255**, 579-602.